

Asteroseismic modelling of *Kepler* Legacy stars including lithium depletion

G. Buldgen^{1,*}, J. Bétrisey², C. Pezzotti¹, S. Borisov³, and A. Noels¹

¹ STAR Institute, University of Liège, 19C Allée du 6 Août, 4000 Liège, Belgium

² Department of Physics and Astronomy, Uppsala University, Box 516, SE-751 20 Uppsala, Sweden

³ Département d'Astronomie, Université de Genève, Chemin Pegasi 51, CH-1290 Versoix, Switzerland

Received 2 July 2025 / Accepted 25 August 2025

ABSTRACT

Context. The *Kepler* Legacy sample is, to this day, the sample of solar-like oscillators with the most exquisite asteroseismic data. In this work, we carry out detailed modelling of a sub-sample of these stars for which the surface lithium abundance has also been observed by the LAMOST survey and a photometric surface rotation has been measured.

Aims. We aim to study the impact of additional mixing processes on the asteroseismic modelling of *Kepler* Legacy G and F-type stars. We also investigate whether a single process can be invoked to reproduce the lithium depletion and asteroseismic constraints at the same time

Methods. We used detailed asteroseismic modelling techniques combining global and local minimisation techniques. We started by using standard models and then aimed to improve this solution with the addition of extra mixing at the border of convective regions using either convective penetration or turbulence in radiative layers.

Results. We find that lower-mass models ($\approx 1 M_{\odot}$) have no problem in reproducing the observed lithium depletion using only turbulence in the radiative zone, similarly to solar models. F-type stars, which have a shallower convective envelope, are unaffected by additional turbulence at the base of the convective zone, but require significant convective penetration values to actually reproduce the observed lithium depletion. The extent of this penetration is, however, incompatible with the frequency separation ratios.

Conclusions. We conclude that the impact of extra mixing is moderate for solar-type stars of the *Kepler* Legacy sample and well within the requirements of the PLATO mission. For more massive stars ($\approx 1.5 M_{\odot}$), we conclude that the behaviour of the frequency separation ratios must be further investigated, as even models with large convective penetration at the base of their convective envelope are unable to reproduce them.

Key words. asteroseismology – stars: abundances – stars: evolution – stars: interiors – stars: solar-type

1. Introduction

Lithium is a key element in stellar evolution. Its low fusion temperature (about 2.5×10^6 K) makes it an extremely sensitive tracer of transport processes happening in stars. Numerous studies have been dedicated to its evolution (e.g. Boesgaard 1976, 1991; Carlos et al. 2019, 2020; Borisov et al. 2024a,b), in an attempt to characterise the underlying physical process at the root of its depletion (e.g. Baglin et al. 1985; Lebreton & Maeder 1987; Montalbán 1994; Charbonnel et al. 1994; Schlattl & Weiss 1999; Montalbán & Schatzman 2000; Thévenin et al. 2017; Baraffe et al. 2017; Eggenberger et al. 2022; Buldgen et al. 2025) as well as its link with the presence of exoplanets (Bouvier 2008; Castro et al. 2009; Deal et al. 2015). It is also a crucial element for primordial nucleosynthesis models (see e.g. Fields 2011; Clara & Martins 2020; Deal & Martins 2021, and refs therein). A critical issue is that lithium, unlike beryllium, is significantly burned during the pre-main-sequence phase, and for a solar-like star its fusion temperature is actually very close to the temperature of the transition between convective and radiative layers. Therefore the observed lithium depletion can be explained by both turbulence in the radiative layers (Dumont et al. 2021b; Eggenberger et al. 2022, e.g. linked with

the transport of angular momentum) or convective undershooting at the base of the convective envelope. In the solar case, it can be shown (see e.g. Buldgen et al. 2025, for a recent study) that turbulence in the radiative zone is required, as significant beryllium depletion is observed at the solar age that can only be reproduced by some mixing quite deep in the radiative zone. However, there is no guarantee that the same processes are acting for other stars, especially as the convective envelope gets thinner with mass.

From the point of view of angular momentum transport, we know that an efficient process should be acting (Aerts et al. 2019), reducing efficiently the effects of shear induced turbulence. While meridional circulation may lead to efficient transport of chemicals, this effect would be directly correlated to the rotation velocity. Another crucial aspect is the actual efficiency of the magnetic braking for stars with thinner envelopes (Matt et al. 2012, 2015; Amard et al. 2016; Matt et al. 2019; Bétrisey et al. 2023b).

On the other hand, F-type stars have recently been shown to present glitches in their frequency separation ratios that can be linked with a significantly deeper position of the base of their convective envelope (Lebreton & Goupil 2012; Deal et al. 2023, 2025). Such extended convective zones would lead to a much higher depletion of lithium and potentially be traceable in a complementary way to detailed seismic modelling.

* Corresponding author: gbuldgen@uliege.be

Table 1. Observational constraints for the stars under study.

Target	$L(L_{\odot})$	T_{eff} (K)	[Fe/H] (dex)	A(Li) (dex)	Rotation Period (P_{Rot}) (d)	Ref.
KIC5773345	5.33 ± 0.19	6204 ± 100	0.28 ± 0.10	2.3 ± 0.1	11.29 ± 0.62	1
KIC5866724	2.68 ± 0.10	6202 ± 80	0.15 ± 0.10	2.95 ± 0.21	$19.56^{+2.24}_{-3.61}$	2
KIC6521045	2.36 ± 0.08	5795 ± 80	0.05 ± 0.10	2.34 ± 0.18	$22.35^{+4.17}_{-2.18}$	2
KIC6679371	7.64 ± 0.31	6379 ± 100	0.00 ± 0.10	3.00 ± 0.11	5.36 ± 0.41	3
KIC7670943	2.78 ± 0.10	6263 ± 100	-0.08 ± 0.10	2.47 ± 0.15	5.14 ± 0.41	2
KIC8292840	2.63 ± 0.09	6357 ± 100	-0.13 ± 0.10	2.66 ± 0.13	$30.10^{+0.54}_{-0.82}$	2
KIC9410862	1.76 ± 0.06	6137 ± 150	-0.36 ± 0.10	2.6 ± 0.16	22.63 ± 1.78	3
KIC10079226	1.53 ± 0.10	5943 ± 100	0.16 ± 0.10	2.55 ± 0.15	15.51 ± 2.35	3
16Cyg A	1.544 ± 0.081	5839 ± 42	0.096 ± 0.026	1.30 ± 0.08	$23.80^{+1.5}_{-1.8}$	4
16Cyg B	1.228 ± 0.064	5809 ± 39	0.052 ± 0.021	0.9	$23.20^{+11.5}_{-3.2}$	4

Notes. (1) Spectroscopic data from Pinsonneault et al. (2012) and seismic data from Lund et al. (2017); (2) Spectroscopic data from Furlan et al. (2018) and seismic data from Davies et al. (2016); (3) Spectroscopic data from Furlan et al. (2018) and seismic data from Lund et al. (2017); (4) T_{eff} from White et al. (2013), [Fe/H] from Ramírez et al. (2009), L from Metcalfe et al. (2012), and seismic data from Davies et al. (2015).

In this study, we analyse a sample of ten solar-like oscillators of G and F spectral type for which high-quality seismic data, surface rotation, and surface lithium abundance have been determined. Our work expands on that of Beck et al. (2017) who focused on solar twins, for most of which only global seismic indicators were available. We carry out a first round of modelling using the FICO procedure defined in Bétrisey et al. (2023a) and use these models as initial conditions for supplementary modelling that attempts to reproduce the lithium depletion. We start by presenting our sample and the constraints we use in Sect. 2. In Sect. 3, we detail our initial modelling approach, and in Sect. 4 we describe the results of the next modelling step, including the observed lithium abundance. Finally, in Sect. 5, we discuss the potential origin of the mixing in the stars of our sample and conclude in Sect. 6 with future prospects and additional studies to be done.

2. Presentation of the sample

We carried out detailed modelling of ten targets for which high-quality asteroseismic data, spectroscopic constraints on lithium, surface rotations, and Gaia parallaxes were available. We summarise these properties in Table 1. The classical constraints used for the seismic modelling were T_{eff} , L , and [Fe/H], except for the 16Cyg binary system, for which we favoured the interferometric radii values from White et al. (2013), $R_A = 1.22 \pm 0.02 R_{\odot}$ and $R_B = 1.12 \pm 0.02 R_{\odot}$.

For 16Cyg A and B, we re-used the set of constraints employed by Bétrisey et al. (2023a). The spectroscopic constraints for KIC5773345 were sourced from Pinsonneault et al. (2012), while those for the remaining targets were obtained from Furlan et al. (2018). The surface rotation periods obtained from photometric analyses were taken from Angus et al. (2018) and Santos et al. (2021). For all targets, we estimated the absolute stellar luminosity using the following formula:

$$\log\left(\frac{L}{L_{\odot}}\right) = -0.4(m_{\lambda} + BC_{\lambda} - 5 \log d + 5 - A_{\lambda} - M_{\text{bol},\odot}), \quad (1)$$

where m_{λ} is the magnitude and λ is the wavelength band, in our case, the 2MASS K_s band. The bolometric correction, BC_{λ} , was computed according to Casagrande & Vandenberg (2014, 2018). For consistency with their software, we adopted a solar bolometric correction of $M_{\text{bol},\odot} = 4.75$. The distance, d , in parsecs is based on Gaia EDR3 (Gaia Collaboration

2021). In that regard, we tested two approaches: using the distance from Bailer-Jones et al. (2021) and inverting the parallax corrected according to Lindegren et al. (2021). For the final luminosity, we adopted the former as both approaches led to consistent luminosities. The extinction, A_{λ} , was inferred using the dust map from Green et al. (2018). We used the seismic data from Davies et al. (2015) for 16Cyg A and B, from Davies et al. (2016) for KIC5866724, KIC6521045, KIC7670943, and KIC8292840, and from Lund et al. (2017) for the remaining targets. For 16Cyg A and B, we used in the modelling the interferometric radius provided by White et al. (2013).

We adopted surface lithium abundances A(Li) from Gao et al. (2021), based on a cross-match of the LAMOST survey with our Kepler sample. For stars with multiple A(Li) measurements in that catalogue (all except for KIC 5773345), we computed a weighted mean using the inverse squared uncertainty as weight. For 16Cyg A and B, we used the reported values in Morel et al. (2021).

3. Asteroseismic modelling using the FICO procedure

The asteroseismic models were constructed using the Forward and Inversion COmbination (FICO) procedure (Bétrisey et al. 2022, 2023a, 2024a; Bétrisey 2024), which combines forward and inverse methods to achieve a detailed stellar characterisation of solar-like stars, based on precursor works by Reese et al. (2012) and Buldgen et al. (2019a). While mixing-length theory is a commonly used approximation for modelling convection (e.g. Maeder 2009; Kippenhahn et al. 2012, for textbooks), including in our study, it has inherent limitations. This theory attempts to describe a complex, non-local 3D turbulent phenomenon using a simplified 1D local approximation that inadequately represents the near-surface layers of stars (e.g. Nordlund & Stein 1997; Stein & Nordlund 1998; Tanner et al. 2013). While this limitation is not critical for stellar physics overall, it becomes significant in asteroseismology because acoustic oscillations originate from these layers. Consequently, the inaccurate treatment of convection introduces biases in the theoretical frequency estimation (e.g. Kjeldsen et al. 2008; Ball & Gizon 2014; Sonoi et al. 2015).

The FICO procedure involves three main steps to construct a model that effectively mitigates these surface effects. From a general perspective, the FICO procedure employs frequency

separation ratios to mitigate surface effects (third step). These ratios are specifically designed to minimise the impact of surface effects (Roxburgh & Vorontsov 2003), albeit at the cost of information about the mean density. This information can be recovered quasi-model-independently through a mean density inversion (second step). We refer to Buldgen et al. (2022a) for a recent review about seismic inversions and briefly note that such techniques were successfully applied to various asteroseismic targets (see e.g. Di Mauro 2004; Buldgen et al. 2016a,b, 2017, 2019a,b, 2022b; Kosovichev & Kitiashvili 2020; Salmon et al. 2021; B  trisey et al. 2022, 2023a,b, 2024a,b, 2025, for a non-exhaustive list of references). Since the mean density inversion relies on a linear formalism to deduce a correction on a so-called reference model (Reese et al. 2012), it must be performed on a model whose reference mean density is sufficiently close to the true mean density in the parameter space. Such a model is obtained by fitting the individual oscillation frequencies and applying a polynomial correction for the surface effects (first step). Although the stellar parameters of this reference model are slightly biased, the reference mean density is close enough to the true value for the inversion to provide a robust and reliable correction.

In practice, the following steps were undertaken. First, we employed the Asteroseismic Inference on a Massive Scale (AIMS) software (Rendle et al. 2019) to fit the individual frequencies and spectroscopic constraints (in our case: effective temperature, metallicity, and luminosity). AIMS employs an MCMC-based algorithm, the Python EMCEE package (Foreman-Mackey et al. 2013), for interpolation between grid points of a pre-computed grid of stellar models, and a Bayesian approach to derive posterior probability distributions of the optimised stellar parameters. The combination of a high-resolution grid with the interpolation scheme allows for a thorough exploration of the parameter space. For the minimisations of this section, we used an extended version of the Spelaion grid from B  trisey et al. (2023a), whose physical ingredients are described in Appendix A. The Spelaion physics will be referred to as standard physics hereafter. Surface effects were modelled using the polynomial prescription of Ball & Gizon (2014). The following stellar variables were optimised in AIMS: mass, age, two mass fractions for the initial chemical composition (X_0 and Z_0), and the two free parameters for the surface effect prescription. For stars with masses exceeding $1.10 M_\odot$, we also included the convective core overshooting parameter in the optimised variables. We employed uniform uninformative priors for all free variables, except for the stellar age, for which we assumed a uniform distribution between 0 and 13.8 Gyr. Observational constraints were assumed to be perturbed by Gaussian-distributed random noise for likelihood computations. The AIMS runs were executed in two phases. Initially, a burn-in phase identified the relevant parameter space, followed by the solution run. For the first minimisation step, we used 800 walkers, 8000 burn-in steps, and 3000 solution steps, resulting in stellar parameters based on 2.4 million samples from the production run, following 6.4 million probability calculations from the burn-in phase. This extensive sampling was feasible due to the limited number of targets in our sample and was required to ensure robust convergence of the surface effect coefficients. Subsequently, a mean density inversion on this reference model was carried out to get a robust constraint on the mean density, which was added to the set of constraints for a second MCMC this time fitting frequency separation ratios instead of individual frequencies. This second AIMS run is based on 2.4 million samples for both the production and solution runs.

Given the potential interpolation challenges when a target is near the end of the main sequence, a region characterised by higher degeneracies in the seismic information (see e.g. White et al. 2011), we conducted an additional test to ensure the robustness of the final step of the FICO procedure. This test involved verifying that the interpolated frequencies from the AIMS solution can be reproduced by recomputing a stellar model using the AIMS optimal parameters and the same versions of the evolution and oscillation codes used for the stellar model grid. A successful interpolation would result in both frequency sets comparably reproducing the observational echelle diagram. Conversely, unsuccessful interpolation would lead to discrepancies in the echelle diagram, indicating that the AIMS interpolated solution is non-physical. Typically, this issue manifests as an overestimation of the stellar age, necessitating a local minimisation to achieve an unbiased stellar characterisation. Although rare, this scenario can occur in regions of the parameter space with higher degeneracy levels. We confirmed the robustness of the interpolation for most targets in our sample, with the exception of KIC6521045. For this target, we performed an additional local minimisation using a Levenberg-Marquardt algorithm (e.g. Frandsen et al. 2002; Teixeira et al. 2003; Miglio & Montalb  n 2005), employing the same free variables as in AIMS. The constraints included the r_{01} frequency separation ratios, the spectroscopic constraints, the inverted mean density, and the lowest radial-order frequency. Since the Levenberg-Marquardt algorithm does not robustly propagate observational uncertainties, we utilised the uncertainties from AIMS. The uncertainty estimation in AIMS is reliable due to the thorough MCMC sampling of the parameter space around the solution, and we assumed that it was reasonable to consider the local minimisation solution sufficiently close to the AIMS solution for reusing this set of uncertainties. We used the asteroseismic models of 16Cyg A and B from B  trisey et al. (2023a). These models were also constructed using the FICO procedure but a better set of constraints could be used for these targets. The asteroseismic modelling results are detailed in Table 2.

4. Modelling including lithium depletion

The second part of our modelling intended to reproduce the observed lithium depletion in these targets while also remaining as consistent as possible with asteroseismic observations. To do this, we considered two distinct physical processes. The first one is turbulent diffusion, modelled as in Proffitt & Michaud (1991) and using the following equation:

$$D_{\text{Turb}} = D_T \left(\frac{\rho_{\text{BCZ}}}{\rho} \right)^n, \quad (2)$$

with ρ_{BCZ} the density at the BCZ position and ρ the local density, D_T and n being the free parameters in this formalism. This empirical approach defines ‘turbulent’ diffusion as a sort of umbrella term that can be linked with various physical processes (see Maeder 2009, for a reference book on instabilities and transport processes). In the following work, we test and compare the required efficiency to reproduce the observed depletion. We note that in the solar case this has been calibrated to simultaneously reproduce the lithium and beryllium abundance (Buldgen et al. 2025) and that attempts to directly link the observed depletion to angular momentum transport processes have been made (Eggenberger et al. 2022), with the beryllium abundance playing a key discriminating role.

The second process is convective undershooting at the base of the envelope. The particularity of lithium is that it is burned

Table 2. Stellar parameters determined from the FICO procedure using standard models.

Target	$M(M_{\odot})$	$R(R_{\odot})$	Age (Gyrs)	X_0	Z_0	α_{Ov}
KIC5773345	1.582 ± 0.026	2.040 ± 0.013	2.14 ± 0.11	0.703	0.028	0.19
KIC5866724	1.298 ± 0.044	1.432 ± 0.017	2.79 ± 0.27	0.697	0.0257	0.03
KIC6521045	1.122 ± 0.080	1.511 ± 0.008	7.38 ± 0.12	0.743	0.0106	0.18
KIC6679371	1.615 ± 0.027	2.246 ± 0.009	1.74 ± 0.08	0.686	0.0247	0.06
KIC7670943	1.235 ± 0.041	1.420 ± 0.016	3.52 ± 0.33	0.733	0.0154	0.07
KIC8292840	1.140 ± 0.030	1.332 ± 0.012	2.75 ± 0.25	0.701	0.0129	0.00
KIC9410862	0.988 ± 0.016	1.159 ± 0.007	6.52 ± 0.42	0.738	0.0082	0
KIC10079226	1.215 ± 0.035	1.178 ± 0.012	2.60 ± 0.30	0.741	0.0209	0.12
16Cyg A	1.057 ± 0.008	1.216 ± 0.005	7.01 ± 0.10	0.708	0.0198	0
16Cyg B	1.010 ± 0.024	1.105 ± 0.009	7.06 ± 0.11	0.711	0.0174	0

Notes. Overshooting has been fixed to 0 for masses below $1.1 M_{\odot}$.

not only during the main sequence but also significantly during the pre-main-sequence evolution. In the early evolutionary phases, the fusion point of lithium is in the convective envelope. As hydrogen burning starts, the convective envelope shrinks and excludes the fusion point of lithium, stopping the depletion. By adding convective undershooting at the base of a convective envelope, one may extend the duration over which the lithium fusion point remains in the convective envelope and the surface abundance is depleted. In our models, we follow a simple formalism of convective penetration for undershooting at the base of the envelope; we shall come back below to our motivations to do so. The equation describing the undershooting parameter is

$$d_{\text{Under}} = \alpha_{\text{Under}} \times H_P, \quad (3)$$

with d_{Under} the distance over which undershooting is acting, α_{Under} a free parameter similar to the mixing-length parameter, and H_P the pressure scale height, defined as $H_P = -\frac{dr}{dmP}$. The mixing in this region is considered instantaneous and the temperature gradient is fixed to the adiabatic gradient. While other prescriptions exist and have been linked with hydrodynamical simulations (e.g. Viallet et al. 2015), asteroseismic data has in some cases shown that strong discontinuities can also be observed at the base of convective envelopes (e.g. Lebreton & Goupil 2012). The ability of undershooting at the base of convective envelopes to be at the root of the observed lithium depletion in solar-like stars has recently been put forward by Baraffe et al. (2017) and Thévenin et al. (2017) and has been mentioned in the solar case in various works (e.g. Christensen-Dalsgaard et al. 2011; Zhang et al. 2019; Dumont et al. 2021a,b).

Due to the lower precision of the lithium abundance determination compared to other observational constraints such as oscillation frequencies, the strategy we adopted was to carry out the modelling without including it explicitly in the cost function, but simply verifying a posteriori that our optimal asteroseismic model actually fell within the 1σ error bar. While slightly more tedious, this also makes the minimisation procedure more stable given the potential degeneracies that may appear should extra mixing be simply treated as a free parameter. This is a consequence of the fact that we model stars presenting only acoustic modes and that we apply a local minimisation technique based on a Levenberg-Marquardt algorithm. The potential weak sensitivity of the acoustic mode to extra mixing (particularly in the form of turbulent diffusion) coupled to the computation of derivatives in the minimisation strategy may lead to convergence issues. Nevertheless we are able to determine for each star a suitable model for the analysis of light element depletion using

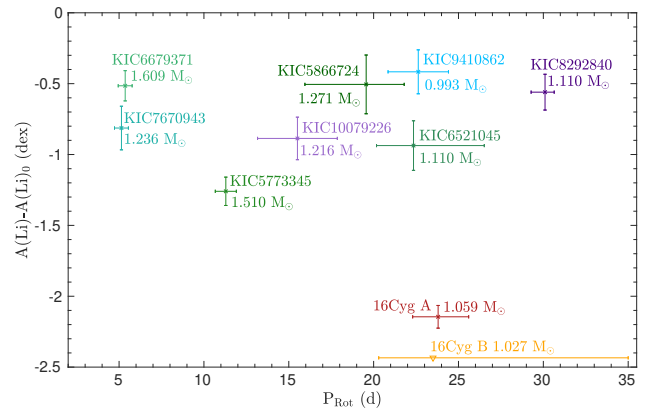


Fig. 1. Surface lithium depletion as a function of surface rotation for all stars in our sample.

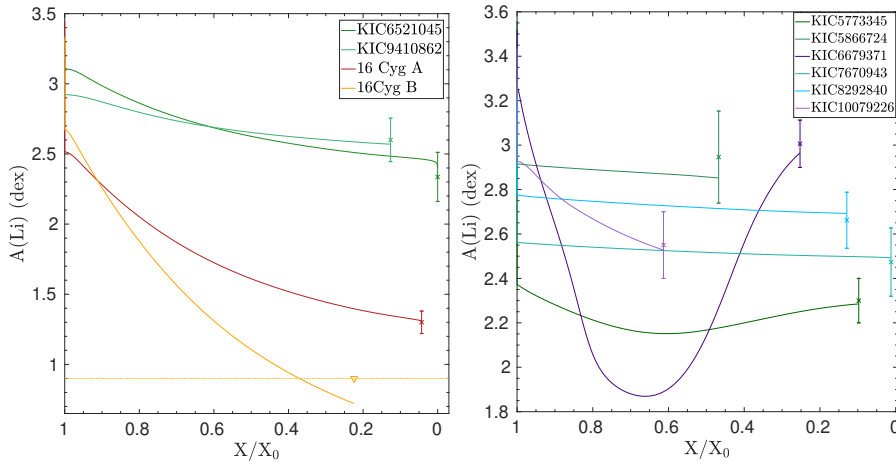
the aforementioned approach. We start by showing in Table 3 the updated parameter values for these stars. As they have been estimated using a local minimisation technique, we discard the uncertainties from the modelling as unreliable and note that the local solution we find would be revised with further revision in the physics. We also note that fitting the r_{01} ratios in some cases leads to more evolved solutions exhibiting negative frequency separation ratios typical of the subgiant branch evolution. These models are discarded as unreliable, as they do not lead to a significantly improved fit but are more a symptom of convergence issues of the method. As we see below, they may result from an attempt of the evolutionary models to fit the frequency separation ratios.

Looking at Fig. 1 and Table 3, we can examine a couple of trends. First, there does not seem to be a direct correlation between the lithium depletion (defined here as $A(\text{Li})-A(\text{Li})_0$, with $A(\text{Li})_0$ the initial surface lithium abundance of the optimal model) and either the rotational velocity or the mass. This is likely a result of the different spectral types in our sample that affect the rotational braking, as a clear correlation is found by Beck et al. (2017). In this respect, the stars of our sample that could be qualified of solar analogues is too small for us to draw any conclusions and consistent modelling of a larger sample should be undertaken, which will likely be possible thanks to the upcoming PLATO mission (Rauer et al. 2024).

For stars such as 16Cyg A, 16Cyg B, KIC9410862, and KIC6521045, classical, moderate turbulence at the BCZ can allow us to reproduce the observed depletion. The efficiency

Table 3. Stellar parameters determined from the local minimisation including light element depletion.

Target	$M(M_{\odot})$	$R(R_{\odot})$	Age (Gyrs)	X_0	Z_0	α_{MLT}	α_{Ov}	α_{Under}	D_T (cm^2/s)	n
KIC5773345	1.510	2.032	2.41	0.69	0.027	1.838	0.01	0.42	10 000	2
KIC5866724	1.271	1.422	2.80	0.707	0.0215	1.701	0.06	0.15	10 000	2
KIC6521045	1.110	1.506	7.18	0.735	0.0121	1.745	0.0	0.0	10 000	2
KIC6679371	1.609	2.234	1.75	0.682	0.0244	1.781	0.05	0.35	10 000	3
KIC7670943	1.236	1.429	3.68	0.731	0.0152	1.973	0.05	0.25	10 000	3
KIC8292840	1.110	1.320	2.82	0.677	0.0122	1.687	0.0	0.30	15 000	2
KIC9410862	0.993	1.160	6.61	0.739	0.0083	1.884	0.0	0.0	3000	3
KIC10079226	1.216	1.177	2.76	0.742	0.0218	1.850	0.14	0.0	10 000	3
16Cyg A	1.059	1.217	7.11	0.702	0.0211	1.843	0.0	0.0	2600	3
16Cyg B	1.027	1.111	7.05	0.726	0.0169	1.842	0.0	0.0	3600	3


Fig. 2. Left panel: Evolution of the surface lithium abundance ($A(\text{Li})$) as a function of central hydrogen abundance (normalised by the initial value) for the lower-mass stars in our sample (G-type stars). The horizontal orange bar indicates the higher limit value for 16Cyg B. Right panel: Same as the left panel, but for the higher-mass stars in our sample (F-type stars) for which undershooting at the base of the convective envelope is necessary to reproduce the surface lithium abundance.

of the turbulent mixing is about 50% lower than the efficiency found by Buldgen et al. (2025) to reproduce the solar lithium and beryllium values when no opacity increase is included. It is, however, in good agreement with the efficiency required in the solar case when an opacity increase at the BCZ is taken into account. This illustrates well the existing correlation between the position of the BCZ and lithium depletion in evolutionary models of solar-like stars and may also imply that some compensation is introduced when carrying out asteroseismic modelling that limits the impact of the reference solar abundances. In the case of 16Cyg, this was already observed in Buldgen et al. (2016a), Farnir et al. (2020) and is further confirmed here.

For all the other stars, despite the fact that the ad hoc turbulence coefficient was set to quite high values (namely $n = 2$ or 3 and $D_T = 10\,000\text{ cm}^2/\text{s}$, or in one case even $15\,000\text{ cm}^2/\text{s}$), it was not possible to reproduce the depletion without undershooting at the base of the convective envelope. We mention that KIC6521045 could fall into this category and that its observed depletion could also easily be reproduced with adiabatic undershooting at the base of the convective envelope and a reduced efficiency of turbulent diffusion.

As can be seen from Fig. 2, this leads to the depletion having a very different shape, reminiscent of the plots in Thévenin et al. (2017), whereas the depletion observed in models including only ad hoc turbulence remains similar to the solar case, as is illustrated in Buldgen et al. (2025). A similar situation has been found in Moedas et al. (2025), where they also found that turbulence in the radiative zone is not sufficient to explain the lithium depletion in their sample of *Kepler* targets. We also note the much steeper depletion of 16Cyg B compared to 16Cyg A,

which indicates either a very different rotational history or, as was put forward by Deal et al. (2015), the impact of a potential early accretion event of a planetary companion. In this case we find that the value of the calibrated turbulent coefficient is 35% higher in 16Cyg B than in 16Cyg A.

Two stars, KIC5773345 and KIC6679371, have peculiarly behaving lithium abundances due to their position at a later stage of hydrogen burning and the combined effect of turbulent diffusion and adiabatic undershooting at the base of the convective envelope. These stars have proven particularly difficult to fit and, as is shown in Fig. 3, their r_{01} ratios (as defined in Roxburgh & Vorontsov 2003) are not at all reproduced. The situation is particularly dire for KIC6679371, despite the solutions being found to be similar to those of the FICO procedure and to those found in the literature (Silva Aguirre et al. 2017). This is in strong contrast with lower-mass G-type stars for which the r_{01} can be matched by the evolutionary models, as is shown in Fig. 4. This indicates an apparent contradiction for both stars, as from their frequency separation ratios one would expect a much deeper convective envelope, as has been confirmed by other studies (Lebreton & Goupil 2012; Deal et al. 2025). However, the lithium depletion is quite moderate compared to the other stars and is reproduced with the calibrated value of undershooting at the base of the convective envelope used in the model.

The higher abundance of lithium is a natural consequence of the evolution, as is illustrated in Fig. 2 for KIC6679371. We see that the deepening of the convective envelope actually leads to an increase in the abundance of lithium, as the convective layers reach regions that are enriched in lithium. Indeed, unlike the case of lower-mass stars, a significant fraction of the radiative layers

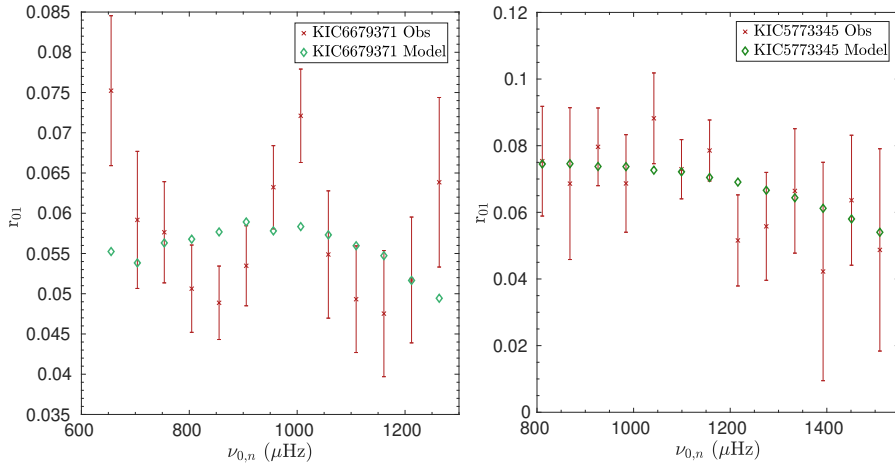


Fig. 3. Frequency separation ratios for the optimal models found after the Levenberg-Marquardt minimisation (r_{01}) of KIC6679371 (left) and KIC5773345 (right) as a function of observed frequency. The evolutionary model is shown in green, while the observations are shown in red.

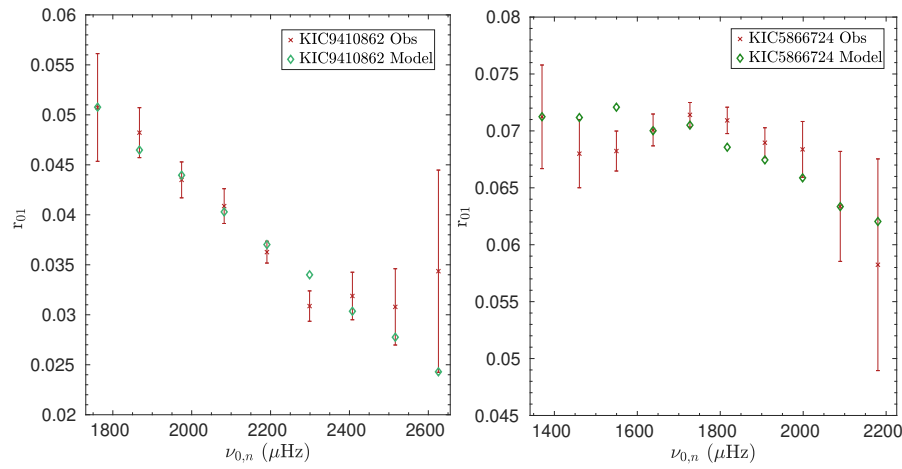


Fig. 4. Frequency separation ratios for the optimal models found after the Levenberg-Marquardt minimisation (r_{01}) of KIC 9410862 (left) and KIC 5866724 (right) as a function of observed frequency. The evolutionary model is shown in green, while the observations are shown in red.

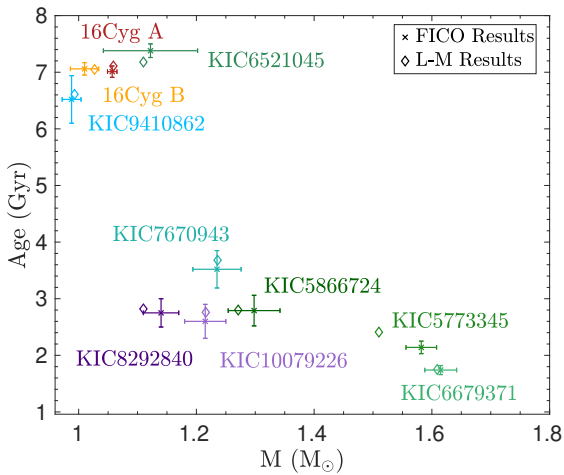


Fig. 5. Variations in the determined astroseismic masses and ages using the FICO procedure and a local Levenberg-Marquardt minimisation that allowed us to reproduce the observed lithium depletion.

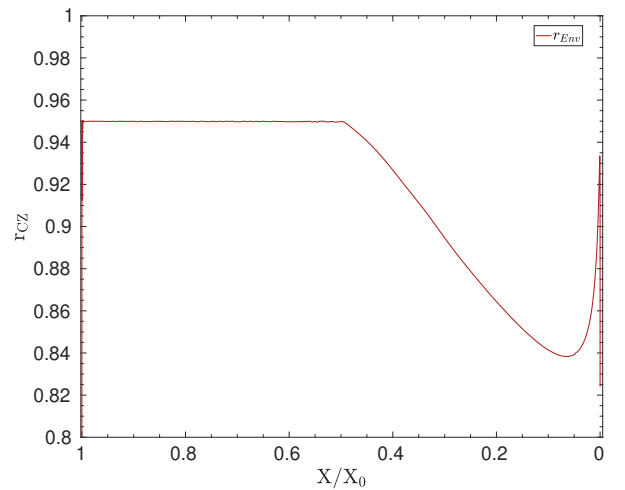


Fig. 6. Evolution of the position of the base of the envelope, r_{Env} , as a function of normalised central hydrogen abundance for the model of KIC6679371.

are too cold to undergo lithium burning. From this behaviour of the higher-mass models close to the turn-off, a potential solution would be to use a slightly more evolved model. The main difficulty would then be keeping the star on the main sequence. In our tests, attempting to reproduce the r_{01} value of KIC6679371 systematically induced our models to evolve on the subgiant branch

and the ratios to become negative, even with high values of adiabatic undershooting at the base of the convective envelope. We come back to this potential solution in Sect. 5. This discrepancy could also be the trace of missing physical ingredients in the evolutionary models we have used, while other explanations may be linked with the actual non-linear response of the frequency

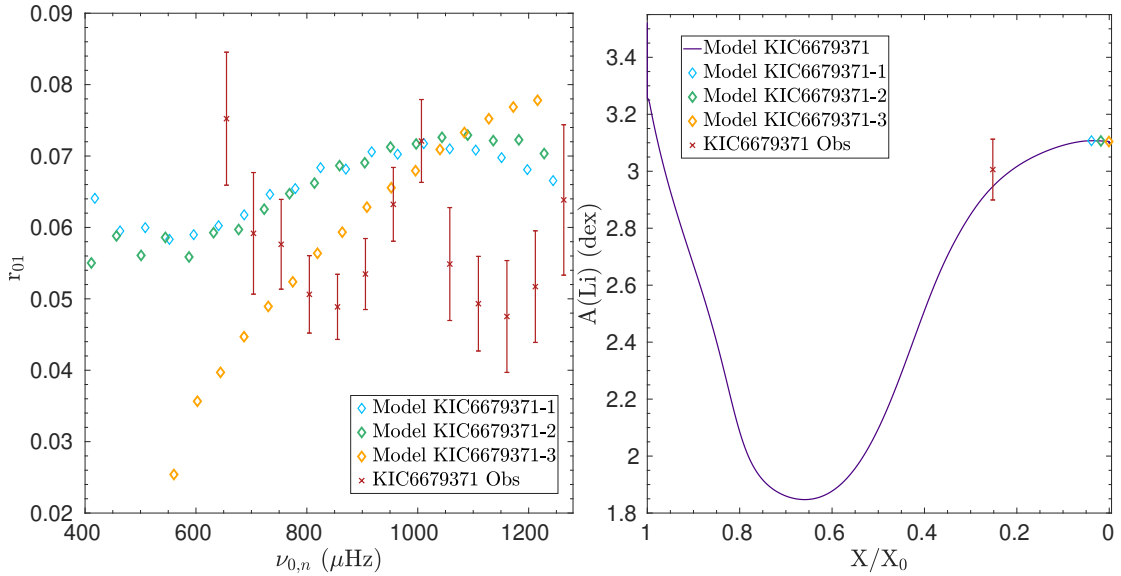


Fig. 7. Left panel: Frequency separation ratios (r_{01}) of KIC6679371 as a function of observed frequency. Right panel: Surface lithium abundance as a function of normalised central hydrogen abundance. The observed value, associated with the X/X_0 from the optimal model, is shown in red. The green, orange, and blue diamonds indicate the positions of Models 1, 2, and 3. Three evolutionary models at the end of the main sequence (denoted Models 1, 2, and 3) are shown.

separation ratios (Deal et al. 2025). In this case, our findings seem to indicate that even directly fitting the ratios without any analytical expression to reproduce the glitch does not allow the models to provide an acceptable agreement and the lithium abundance of these stars confirms that they should be close to the end of the main sequence. This work thus motivates further theoretical investigations to explain the observed differences and the reason why evolutionary models are unable to reproduce the data.

In our current modelling, the shifts in mass and age from the inclusion of the lithium depletion and variation in the transport of chemicals in the models remain minute, but further investigation is required as solutions aiming to reproduce the r_{01} for KIC6679371 tend to go as low as $1.4 M_{\odot}$, and thus a change of about 15%. For solar-like stars, the changes remain minute and well within the requirements of the PLATO mission. This is illustrated in Fig. 5 for all targets of the sample. A clear trend is observed, with the more massive stars showing larger deviations. We stress that these values remain lower estimates of the possible shifts, given that the agreement with seismic indicators is not yet satisfactory in some cases and requires further theoretical investigations. It is also likely that the effects of radiative accelerations or calibrated values of convective core overshooting from numerical simulations will impact the higher-mass solutions, particularly KIC6679371 and KIC5773345.

Comparing the variations in Fig. 5, however, only tells one part of the story. Looking at the α_{MLT} or α_{Ov} parameters in Tables 2 and 3, we find more significant discrepancies between the two solutions. It is, however, difficult to come to any quantitative conclusions about their validity, and while departures from the solar calibrated value of α_{MLT} used for the grid in the FICO procedure are expected, we cannot safely exclude compensations. For example, it is likely that the reduction in the efficiency of settling resulting from the added turbulence in the radiative zone to reproduce lithium induced a variation in α_{MLT} and α_{Ov} to restore the agreement with seismic and classical constraints. Further tests using entropy-calibrated as in Manchon et al. (2024) might help, although they are unlikely to explain the discrepancies discussed above for KIC6679371 and KIC5773345.

5. Attempting to reconcile the frequency separation ratios and the lithium abundance

As was mentioned above, the situation observed in the case of KIC6679371 and KIC5773345 is quite peculiar, as the BCZ position will naturally extend deeper in the model, while the lithium abundance will increase and finally form a plateau. This is linked to the convective envelope reaching deeper regions in the star, yet unaffected by lithium combustion. This is illustrated in Fig. 6, where we show that towards the second half of the MS, the envelope deepens as the convective core shrinks. This is in line with the renewed increase of the lithium that we see in the right panel of Fig. 2. We note, however, that there is an effect of turbulent diffusion, as both the decrease and increase in the surface lithium abundance are not fully linked with the BCZ position. Indeed, significant burning still occurs during the main sequence under the effect of turbulent diffusion, which is enhanced by the extension of the convective envelope using undershooting at its lower boundary.

We show in Fig. 7 the evolution of the surface lithium abundance for a model evolved beyond the ‘optimal age’ found for KIC6679371, as well as a few examples of frequency separation ratios, for the observed modes. Given that it forms a plateau towards the end of the main sequence, lithium is essentially uninformative about the actual age of the star as soon as the convective envelope expands. Regarding the frequency separation ratios, illustrated in the left panel of Fig. 7, we can see that letting the model evolve further is not the solution, at least not at a fixed mass. None of the models exhibit the high-amplitude glitches observed in the r_{01} ratios of KIC6679371, despite the BCZ being 5% deeper than in the optimal model, which appears largely insufficient. Moreover, the slope of the r_{01} ratios as a function of frequency remains sensitive to the core properties. We can observe a rapid and drastic increase, in contradiction with the behaviour in the observations and in main-sequence models that exhibit either a rather flat frequency dependency or a negative slope of the r_{01} separation ratios. This is mostly seen in stars close to the subgiant branch and it is expected that the

r_{01} will take negative values (White et al. 2011; Deheuvels et al. 2016). This was actually seen for the third model that exhibits a steep slope in the low-frequency regime due to the core contraction in this model.

This implies that on top of the BCZ having to be significantly deeper, the core properties, to which the slope of the r_{01} ratios remains sensitive, must be those of a main-sequence star. This further complicates the analysis and requires more detailed investigations, likely with a different optimisation technique than the Levenberg-Marquardt approach used here.

6. Conclusions

In this paper, we have carried out a detailed modelling procedure of ten targets in the *Kepler* Legacy sample for which a spectroscopic measurement of the surface lithium abundance was available. We have presented in Sect. 2 the sample of stars we studied and the determination of the luminosity using spectroscopic constraints and Gaia parallaxes. In Sect. 3, we have presented the results obtained from the modelling using the FICO procedure (B  trisey et al. 2023a). These values constitute updated reference parameters for these targets using the most recent modelling strategies and updated physical ingredients regarding previous studies in the literature. However, as they did not include the lithium depletion, we carried out dedicated modelling of the targets using asteroseismic constraints and aiming to add either turbulence or undershooting at the base of the convective envelope to reproduce the observed lithium depletion. The results of this modelling were presented in Sect. 4 and show in general relatively minor modifications from the ones obtained from the FICO procedure. From this analysis, we found that for the G-type, lower-mass stars in our sample the lithium depletion could easily be reproduced by adding a turbulent diffusion at the base of the convective envelope, similarly to what is done in the solar case. Meanwhile, for the more massive stars of our sample, even pushing to higher values of this ad hoc turbulent diffusion was insufficient to reduce the surface lithium abundance. We found that this is a direct consequence of the very shallow convective zone that these stars exhibit, meaning that extending the convective envelope was required to reproduce the observed lithium abundance.

By adding undershooting at the base of the convective envelope, we are able to deplete lithium in the early main sequence and reproduce the observed values. While this provides a good fit of the r_{01} frequency separation ratios, we find that in some specific cases, namely KIC6679371 and KIC5773345, the lithium abundance is too high with respect to the required undershooting at the base of the convective envelope to reproduce the frequency separation ratios. While this is not in disagreement with evolutionary model predictions, as the lithium abundance in this mass range is expected to increase again at the end of the main sequence, the observed signature in the ratios cannot be reproduced by simply pushing the models to a slightly higher age, as is shown in Sect. 5. Our results confirm the investigations of Deal et al. (2023) and Deal et al. (2025) and may imply that either the evolutionary solution is not reachable in our models because of missing physical ingredients or the behaviour of the modes is not properly described with our oscillation codes. The modelling of convection by the mixing length theory used in the evolutionary models might not be suitable in such thin convective envelopes. It is therefore possible that the observed behaviour here for pressure modes is a result of a stronger coupling between oscillations and convection. Issues with the treatment of time-dependent convection and turbulence models have

also been cited as explanations for the difficulties in reproducing the γ Doradus instability strip (Dupret et al. 2005), which lies in a similar mass range as KIC6679371 and KIC5773345. This also implies that lithium might not be a good calibrator of turbulent mixing in F-type stars as its depletion could be due to, or even require, undershooting at the base of the convective envelope. Fortunately, signatures on the helium abundance in the convective envelope may provide a calibration of turbulent transport (Verma & Silva Aguirre 2019). Further theoretical investigations on the behaviour of the frequency separation ratios are required for us to reach a conclusion in one direction or the other. This, however, puts some suspicion on the inferred masses and ages in this mass range and especially the values of KIC6679371 and KIC5773345 reported here.

Future investigations are required to optimally exploit the seismic data provided by the PLATO mission (Rauer et al. 2024) and to define robust modelling strategies for these targets that may be a significant fraction of the main PLATO sample (Goupil et al. 2024). At first, a better understanding of the observed asteroseismic signatures, in line with the works of Deal et al. (2025), will be crucial to interpret these observations. Finally, our findings also imply that testing fundamental physics ingredients might require more advanced numerical schemes than Levenberg-Marquardt algorithms, even though a first round of MCMC modelling has been carried out. This is particularly true for stars close to the turn-off that may display strong non-linear behaviours.

Acknowledgements. We thank the referee for their careful reading of the manuscript and insightful comments. G.B. acknowledges fundings from the Fonds National de la Recherche Scientifique (FNRS) as a postdoctoral researcher. J.B. acknowledges funding from the SNF Postdoc.Mobility grant no. P500PT_222217 (Impact of magnetic activity on the characterisation of FGKM main-sequence host-stars). We are grateful to Saniya Khan for her help with the determination of the luminosity and the use of the extinction and bolometric correction softwares. We thank Morgan Deal for the fruitful discussions on the issues linked with the ratios of F-type stars and particularly of KIC6679371.

References

- Adelberger, E. G., Garc  a, A., Robertson, R. G. H., et al. 2011, *Rev. Mode. Phys.*, **83**, 195
- Aerts, C., Mathis, S., & Rogers, T. M. 2019, *ARA&A*, **57**, 35
- Amard, L., Palacios, A., Charbonnel, C., Gallet, F., & Bouvier, J. 2016, *A&A*, **587**, A105
- Angus, R., Morton, T., Aigrain, S., Foreman-Mackey, D., & Rajpaul, V. 2018, *MNRAS*, **474**, 2094
- Baglin, A., Morel, P. J., & Schatzman, E. 1985, *A&A*, **149**, 309
- Bailer-Jones, C. A. L., Rybizki, J., Fousneau, M., Demleitner, M., & Andrae, R. 2021, *AJ*, **161**, 147
- Ball, W. H., & Gizon, L. 2014, *A&A*, **568**, A123
- Baraffe, I., Pratt, J., Goffrey, T., et al. 2017, *ApJ*, **845**, L6
- Beck, P. G., do Nascimento, J. D., Jr., Duarte, T., et al. 2017, *A&A*, **602**, A63
- B  trisey, J. 2024, Ph.D. Thesis, University of Geneva, Switzerland
- B  trisey, J., Pezzotti, C., Buldgen, G., et al. 2022, *A&A*, **659**, A56
- B  trisey, J., Buldgen, G., Reese, D. R., et al. 2023a, *A&A*, **676**, A10
- B  trisey, J., Eggenberger, P., Buldgen, G., Benomar, O., & Bazot, M. 2023b, *A&A*, **673**, L11
- B  trisey, J., Buldgen, G., Reese, D. R., & Meynet, G. 2024a, *A&A*, **681**, A99
- B  trisey, J., Farnir, M., Breton, S. N., et al. 2024b, *A&A*, **688**, L17
- B  trisey, J., Reese, D. R., Breton, S. N., et al. 2025, *A&A*, **697**, A219
- Boesgaard, A. M. 1976, *PASP*, **88**, 353
- Boesgaard, A. M. 1991, *ApJ*, **370**, L95
- Borisov, S., Charbonnel, C., Prantzos, N., Dumont, T., & Palacios, A. 2024a, *A&A*, **690**, A245
- Borisov, S., Prantzos, N., & Charbonnel, C. 2024b, *A&A*, **691**, A142
- Bouvier, J. 2008, *A&A*, **489**, L53
- Buldgen, G., Reese, D. R., & Dupret, M. A. 2016a, *A&A*, **585**, A109
- Buldgen, G., Salmon, S. J. A. J., Reese, D. R., & Dupret, M. A. 2016b, *A&A*, **596**, A73

- Buldgen, G., Reese, D., & Dupret, M.-A. 2017, *Eur. Phys. J. Web Conf.*, **160**, 03005
- Buldgen, G., Farnir, M., Pezzotti, C., et al. 2019a, *A&A*, **630**, A126
- Buldgen, G., Rendle, B., Sonoï, T., et al. 2019b, *MNRAS*, **482**, 2305
- Buldgen, G., Bétrisey, J., Roxburgh, I. W., Vorontsov, S. V., & Reese, D. R. 2022a, *Front. Astron. Space Sci.*, **9**, 942373
- Buldgen, G., Farnir, M., Eggenberger, P., et al. 2022b, *A&A*, **661**, A143
- Buldgen, G., Noels, A., Amarsi, A. M., et al. 2025, *A&A*, **694**, A285
- Carlos, M., Meléndez, J., Spina, L., et al. 2019, *MNRAS*, **485**, 4052
- Carlos, M., Meléndez, J., do Nascimento, J. D., & Castro, M. 2020, *MNRAS*, **492**, 245
- Casagrande, L., & VandenBerg, D. A. 2014, *MNRAS*, **444**, 392
- Casagrande, L., & VandenBerg, D. A. 2018, *MNRAS*, **475**, 5023
- Castro, M., Vauclair, S., Richard, O., & Santos, N. C. 2009, *A&A*, **494**, 663
- Charbonnel, C., Vauclair, S., Maeder, A., Meynet, G., & Schaller, G. 1994, *A&A*, **283**, 155
- Christensen-Dalsgaard, J., Monteiro, M. J. P. F. G., Rempel, M., & Thompson, M. J. 2011, *MNRAS*, **414**, 1158
- Clara, M. T., & Martins, C. J. A. P. 2020, *A&A*, **633**, L11
- Cox, J. P., & Giuli, R. T. 1968, *Principles of Stellar Structure* (Gordon and Breach)
- Davies, G. R., Chaplin, W. J., Farr, W. M., et al. 2015, *MNRAS*, **446**, 2959
- Davies, G. R., Silva Aguirre, V., Bedding, T. R., et al. 2016, *MNRAS*, **456**, 2183
- Deal, M., & Martins, C. J. A. P. 2021, *A&A*, **653**, A48
- Deal, M., Richard, O., & Vauclair, S. 2015, *A&A*, **584**, A105
- Deal, M., Goupil, M. J., Cunha, M. S., et al. 2023, *A&A*, **673**, A49
- Deal, M., Goupil, M. J., Philidet, J., et al. 2025, *A&A*, **693**, A240
- Deheuvels, S., Brandão, I., Silva Aguirre, V., et al. 2016, *A&A*, **589**, A93
- Di Mauro, M. P. 2004, in *SOHO 14 Helio- and Asteroseismology: Towards a Golden Future*, ed. D. Danesy, *ESA Spec. Pub.*, **559**, 186
- Dumont, T., Charbonnel, C., Palacios, A., & Borisov, S. 2021a, *A&A*, **654**, A46
- Dumont, T., Palacios, A., Charbonnel, C., et al. 2021b, *A&A*, **646**, A48
- Dupret, M. A., Grigahcène, A., Garrido, R., Gabriel, M., & Scuflaire, R. 2005, *A&A*, **435**, 927
- Eggenberger, P., Buldgen, G., Salmon, S. J. A. J., et al. 2022, *Nat. Astron.*, **6**, 788
- Farnir, M., Dupret, M. A., Buldgen, G., et al. 2020, *A&A*, **644**, A37
- Ferguson, J. W., Alexander, D. R., Allard, F., et al. 2005, *ApJ*, **623**, 585
- Fields, B. D. 2011, *Ann. Rev. Nucl. Part. Sci.*, **61**, 47
- Foreman-Mackey, D., Hogg, D. W., Lang, D., & Goodman, J. 2013, *PASP*, **125**, 306
- Frandsen, S., Carrier, F., Aerts, C., et al. 2002, *A&A*, **394**, L5
- Furlan, E., Ciardi, D. R., Cochran, W. D., et al. 2018, *ApJ*, **861**, 149
- Gaia Collaboration (Brown, A. G. A., et al.) 2021, *A&A*, **649**, A1
- Gao, Q., Shi, J.-R., Yan, H.-L., et al. 2021, *ApJ*, **914**, 116
- Goupil, M. J., Catala, C., Samadi, R., et al. 2024, *A&A*, **683**, A78
- Green, G. M., Schlafly, E. F., Finkbeiner, D., et al. 2018, *MNRAS*, **478**, 651
- Iglesias, C. A., & Rogers, F. J. 1996, *ApJ*, **464**, 943
- Irwin, A. W. 2012, *FreeEOS: Equation of State for stellar interiors calculations*
- Kippenhahn, R., Weigert, A., & Weiss, A. 2012, *Stellar Structure and Evolution, Astronomy and Astrophysics Library* (Berlin Heidelberg: Springer)
- Kjeldsen, H., Bedding, T. R., & Christensen-Dalsgaard, J. 2008, *ApJ*, **683**, L175
- Kosovichev, A. G., & Kitiashvili, I. N. 2020, in *Solar and Stellar Magnetic Fields: Origins and Manifestations*, eds. A. Kosovichev, S. Strassmeier, & M. Jardine, 354, 107
- Lebreton, Y., & Goupil, M. J. 2012, *A&A*, **544**, L13
- Lebreton, Y., & Maeder, A. 1987, *A&A*, **175**, 99
- Lindegren, L., Bastian, U., Biermann, M., et al. 2021, *A&A*, **649**, A4
- Lund, M. N., Silva Aguirre, V., Davies, G. R., et al. 2017, *ApJ*, **835**, 172
- Maeder, A. 2009, *Physics, Formation and Evolution of Rotating Stars* (Springer Verlag)
- Manchon, L., Deal, M., Goupil, M. J., et al. 2024, *A&A*, **687**, A146
- Matt, S. P., MacGregor, K. B., Pinsonneault, M. H., & Greene, T. P. 2012, *ApJ*, **754**, L26
- Matt, S. P., Brun, A. S., Baraffe, I., Bouvier, J., & Chabrier, G. 2015, *ApJ*, **799**, L23
- Matt, S. P., Brun, A. S., Baraffe, I., Bouvier, J., & Chabrier, G. 2019, *ApJ*, **870**, L27
- Metcalfe, T. S., Chaplin, W. J., Appourchaux, T., et al. 2012, *ApJ*, **748**, L10
- Miglio, A., & Montalbán, J. 2005, *A&A*, **441**, 615
- Moedas, N., Deal, M., & Bossini, D. 2025, *A&A*, **695**, A9
- Montalbán, J. 1994, *A&A*, **281**, 421
- Montalbán, J., & Schatzman, E. 2000, *A&A*, **354**, 943
- Morel, T., Creevey, O. L., Montalbán, J., Miglio, A., & Willett, E. 2021, *A&A*, **646**, A78
- Nordlund, A., & Stein, R. 1997, in *SCORE'96 : Solar Convection and Oscillations and their Relationship*, eds. F. P. Pijpers, J. Christensen-Dalsgaard, & C. S. Rosenthal, *Astrophys. Space Sci. Lib.*, **225**, 79
- Paquette, C., Pelletier, C., Fontaine, G., & Michaud, G. 1986, *ApJS*, **61**, 177
- Pinsonneault, M. H., An, D., Molenda-Żakowicz, J., et al. 2012, *ApJS*, **199**, 30
- Potekhin, A. Y., Baiko, D. A., Haensel, P., & Yakovlev, D. G. 1999, *A&A*, **346**, 345
- Proffitt, C. R., & Michaud, G. 1991, *ApJ*, **380**, 238
- Ramírez, I., Meléndez, J., & Asplund, M. 2009, *A&A*, **508**, L17
- Rauer, H., Aerts, C., Cabrera, J., et al. 2024, arXiv e-prints [arXiv:2406.05447]
- Reese, D. R., Marques, J. P., Goupil, M. J., Thompson, M. J., & Deheuvels, S. 2012, *A&A*, **539**, A63
- Rendle, B. M., Buldgen, G., Miglio, A., et al. 2019, *MNRAS*, **484**, 771
- Rogers, F. J., & Nayfonov, A. 2002, *ApJ*, **576**, 1064
- Roxburgh, I. W., & Vorontsov, S. V. 2003, *A&A*, **411**, 215
- Salmon, S. J. A. J., Van Grootel, V., Buldgen, G., Dupret, M. A., & Eggenberger, P. 2021, *A&A*, **646**, A7
- Santos, A. R. G., Breton, S. N., Mathur, S., & García, R. A. 2021, *ApJS*, **255**, 17
- Schlattl, H., & Weiss, A. 1999, *A&A*, **347**, 272
- Scuflaire, R., Montalbán, J., Théado, S., et al. 2008a, *Ap&SS*, **316**, 149
- Scuflaire, R., Théado, S., Montalbán, J., et al. 2008b, *Ap&SS*, **316**, 83
- Silva Aguirre, V., Lund, M. N., Antia, H. M., et al. 2017, *ApJ*, **835**, 173
- Sonoï, T., Samadi, R., Belkacem, K., et al. 2015, *A&A*, **583**, A112
- Stein, R. F., & Nordlund, Å. 1998, *ApJ*, **499**, 914
- Tanner, J. D., Basu, S., & Demarque, P. 2013, *ApJ*, **767**, 78
- Teixeira, T. C., Christensen-Dalsgaard, J., Carrier, F., et al. 2003, *Ap&SS*, **284**, 233
- Thévenin, F., Oreshina, A. V., Baturin, V. A., et al. 2017, *A&A*, **598**, A64
- Thoul, A. A., Bahcall, J. N., & Loeb, A. 1994, *ApJ*, **421**, 828
- Verma, K., & Silva Aguirre, V. 2019, *MNRAS*, **489**, 1850
- Vernazza, J. E., Avrett, E. H., & Loeser, R. 1981, *ApJS*, **45**, 635
- Viallet, M., Meakin, C., Prat, V., & Arnett, D. 2015, *A&A*, **580**, A61
- White, T. R., Bedding, T. R., Stello, D., et al. 2011, *ApJ*, **743**, 161
- White, T. R., Huber, D., Maestro, V., et al. 2013, *MNRAS*, **433**, 1262
- Zhang, Q.-S., Li, Y., & Christensen-Dalsgaard, J. 2019, *ApJ*, **881**, 103

Appendix A: The Spelaion physics

The Spelaion grid comprises several subgrids, each designed to model specific types of stellar physics (see [Bétryse et al. 2023a](#)). In Sect. 3, we utilised two subgrids, labelled as ‘Standard MS’ and ‘Overshooting MS’ in [Bétryse et al. \(2023a\)](#). The Standard MS subgrid has a convective core overshooting parameter fixed at zero, while the Overshooting MS subgrid includes the core overshooting parameter as a free variable. We note that these two subgrids have been extended to cover slightly larger masses and lower metallicities since the publication of the [Bétryse et al. \(2023a\)](#) paper, which is why we refer to the extended Spelaion grid in the main text.

The evolutionary sequences of the subgrids were computed using the Liège evolution code (CLES; [Scuflaire et al. 2008b](#)). For each model in the sequence, the adiabatic Liège oscillation code (LOSC; [Scuflaire et al. 2008a](#)) was used to compute the acoustic oscillation frequencies. The stellar models incorporate AGSS09 abundances ([Asplund et al. 2009](#)) and OPAL opacities ([Iglesias & Rogers 1996](#)), supplemented by [Ferguson et al. \(2005\)](#) opacities at low temperatures and electron conductivity by [Potekhin et al. \(1999\)](#). The equation of state is described by the FreeEOS equation of state ([Irwin 2012](#)), and it is worth noting that the OPAL opacities are based on the OPAL2005 equation of state ([Rogers & Nayfonov 2002](#)). We employed the [Thoul et al. \(1994\)](#) formalism for microscopic diffusion, with the screening coefficients of [Paquette et al. \(1986\)](#). The nuclear reaction rates were sourced from [Adelberger et al. \(2011\)](#). Convection was modelled using the mixing-length theory from [Cox & Giuli \(1968\)](#), with a mixing-length parameter α_{MLT} fixed at a solar-calibrated value of 2.05. We used the $T(\tau)$ relation from model C of [Vernazza et al. \(1981\)](#) for atmospheric modelling.